Military Technical College
Kobry El-Kobba
Cairo, Egypt

12-th International Conference
on
Aerospace Sciences &
Aviation Technology

ON THE NUMERICAL SOLUTION OF THE INVISCID TWO DIMENSIONAL INTERNAL FLOWS WITH NON-ORTHOGONAL GRIDS

Mohammad Baher Azab* , M.M. Abdelrahman** and M. I. Mostafa*

ABSTRACT

A new boundary condition treatment strategy is presented in this research for solving the two-dimensional inviscid internal flow problems, spatial discretization has made by finite difference formulation using flux vector splitting of Van Leer. The time advancement is made using Euler backward time stepping technique. The aim of this research is to present new non-reflecting boundary condition treatment in the cases of metaphysical flow conditions occurred at the same space point. Such situation occurred in the internal flow problems as the corner points in nozzle., numerical flow simulations is carried out and shows good agreement with the analytical values and with published data.

NOMENCLATURE

CFL	Courant number
e_{tt}	Total energy.
a	Speed of sound.
γ	Specific heat ratio
ρ	Static density.
P	Static pressure.
u, v	Cartesian velocity components
U, V	Contravariant velocity components
J	Jacobian.
M	Mach number.
x, y	Physical plane coordinates.
ξ, η	Computational plane coordinates.
ΔQ	Increment in conservative variables
Λ	Eigenvalues diagonal matrix.
ξ_t, ξ_x, ξ_y	$\frac{\partial \xi}{\partial t}, \frac{\partial \xi}{\partial x}, \frac{\partial \xi}{\partial y}$
η_t, η_x, η_y	$\frac{\partial \eta}{\partial t}, \frac{\partial \eta}{\partial x}, \frac{\partial \eta}{\partial y}$

* Egyptian Armed Forces
** Professor, Aerospace engineering department, Cairo University, Cairo, Egypt

INTRODUCTION

The goal of this research is to implement a new mathematical boundary condition treatment to solve internal flow problems for subsonic, transonic, and supersonic flow regimes. The proposed method is applied to solve the compressible inviscid flow through Nozzles and turbomachines. The computational model, based on the flux vector splitting technique, is used to solve the unsteady two-dimensional Euler equations.

The Van Leer and Steger-Warming flux vector splitting methods are adopted for solving the system of governing equations. A special mathematical treatment is proposed that handle combinations of the flow boundary conditions. The developed Solver is applied to solve the two-dimensional subsonic, transonic, and supersonic flows through nozzles. The results show the capability of the code to present fast and accurate solutions using non-orthogonal grid at the boundary surface. A sharp resolution of the curved shock wave location is observed. The grid spacing normal to the boundary surface and achieved in this study was estimated to be fifty times larger than the recommended values by some researchers. The previous achievement leads to a substantial saving in computer memory and reduction in the number of grid points with reasonable accuracy and stability of the solution.

Another version of the two-dimensional code was developed to solve subsonic and transonic two-dimensional cascade flow. A comparison with published experimental data is carried out and good agreement is noticed.

Governing Equations

The implemented flow model is Euler's model, which represents the conservation of mass and balance of momentum and energy and contains the effect of rotationality associated with the formation of shock waves in compressible flow field. The flow field variables are nondimensionalized as follows:

$$\rho = \frac{\tilde{\rho}}{\rho_o} \quad u = \frac{\tilde{u}}{a_o} \quad v = \frac{\tilde{v}}{a_o} \quad w = \frac{\tilde{w}}{a_o} \quad p = \frac{\tilde{p}}{\rho_o a_o^2} \quad e_{tt} = \frac{\tilde{e}_{tt}}{\rho_o a^2{}_o} \quad a = \frac{\tilde{a}}{a_o} \quad x = \frac{\tilde{x}}{l_r} \quad y = \frac{\tilde{y}}{l_r}$$

$$z = \frac{\tilde{z}}{l_r} \quad t = \frac{\tilde{t}^* a_o}{l_r}$$

The governing equations written in the computational plane;

$$\frac{\partial Q}{\partial t} + \frac{\partial E}{\partial \varsigma} + \frac{\partial F}{\partial \eta} = 0$$

$$Q = \frac{1}{J}\begin{bmatrix} \rho \\ \rho.u \\ \rho.v \\ \rho.e_t \end{bmatrix}, E = \begin{bmatrix} \rho.U \\ \rho.u.U + \varsigma_x.p \\ \rho.v.U + \varsigma_y.p \\ U.(\rho.e_t + p) \end{bmatrix}, F = \begin{bmatrix} \rho.V \\ \rho.u.V + \eta_x.p \\ \rho.v.V + \eta_y.p \\ V.(\rho.e_t + p) \end{bmatrix} \qquad (1)$$

where

$$U = \varsigma_t + \varsigma_x.u + \varsigma_y.v$$
$$V = \eta_t + \eta_x.u + \eta_y.v$$
$$J = \varsigma_x.\eta_y - \varsigma_y.\eta_x = \frac{1}{x_\varsigma.y_\eta - x_\eta.y_\varsigma}$$

$$\varsigma_x = J.y_\eta \qquad \varsigma_y = -J.x_\eta$$
$$\eta_x = J.y_\varsigma \qquad \eta_y = -J.x_\varsigma \tag{2}$$

Numerical Procedure

The governing equations are descretised on finite difference formulation where the spatial derivatives are evaluated using Van Leer flux vector splitting technique.
The descretised flow equations suitable for implicit time marching can be written as;

$$\left[I + \Delta t * \left(\frac{\partial A}{\partial \xi} + \frac{\partial B}{\partial \eta}\right)\right]\Delta Q = -\Delta t * \left(\frac{\partial E}{\partial \xi} + \frac{\partial F}{\partial \eta}\right)^n \tag{3}$$

where

$$A = \frac{\partial E^n}{\partial Q} \qquad B = \frac{\partial F^n}{\partial Q} \tag{4}$$
$$\Delta Q = Q^{n+1} - Q^n$$

The generalized fluxes $\hat{E}$ and $\hat{F}$ are split into forward and backward contributions according to the signs of the eigenvalues of the associated Jacobian matrices, $\frac{\partial E}{\partial Q}, \frac{\partial F}{\partial Q}$, and are differenced accordingly.
The flux in the ξ and η-directions can be differenced as:

$$\delta_\varsigma E = \delta_\varsigma^- E^+ + \delta_\varsigma^+ E^- \tag{5}$$

$$\delta_\eta F = \delta_\eta^- F^+ + \delta_\eta^+ F^- \tag{6}$$

Where E^+ and F^+ has all positive eigenvalues and E^- and F^- has all negative eigenvalues.
The Van Leer flux-vector splitting, E is split according to the contravariant Mach number in the ξ direction, defined as:

$$M_\xi = \frac{\bar{U}}{a} \tag{7}$$
$$\bar{U} = \frac{U}{|\nabla \xi|} \tag{8}$$

and

$$U = \xi_x u + \xi_y v + \xi_t \tag{9}$$

For locally supersonic flow, where $\left|M_\xi\right| \geq 1$,

E^+=E. E^-=0. $M_\xi \geq +1$

E^-=E. E^+=0. $M_\xi \leq -1$ (10)

For locally subsonic flow $\left|M_\xi\right| < 1$ the Flux and Jacobian matrix are

$$E^\pm = \frac{|\nabla\xi|}{J}\begin{bmatrix} f^\pm_{mass} \\ f^\pm_{mass}\left[\hat{\xi}_x\left(-\bar{U} \pm a\right)/\gamma + u\right] \\ f^\pm_{mass}\left[\hat{\xi}_z\left(-\bar{U} \pm a\right)/\gamma + w\right] \\ f^\pm_{energy} \end{bmatrix} \tag{11}$$

where

$$\xi_x = \frac{\xi_x}{|\nabla\xi|} \qquad \xi_y = \frac{\xi_y}{|\nabla\xi|} \tag{12}$$

and

$$f^\pm_{mass} = \pm\frac{\rho a}{4}\left(M_\xi \pm 1\right)^2$$

$$f^\pm_{energy} = f^\pm_{mass}\left[\frac{(1-\gamma)\bar{U}^2 \pm 2(\gamma-1)\bar{U}a + 2a^2}{(\gamma^2-1)} + \frac{\left(u^2+v^2\right)}{2} - \frac{\xi_t}{\gamma}\left(-\bar{U} \pm 2a\right)\right] \tag{13}$$

and

$$\xi_t = \frac{\xi_t}{|\nabla\xi|} \tag{14}$$

The Jacobian matrices $A^\pm = \frac{\partial E^\pm}{\partial Q}$ can be expressed using MapleV symbolic manipulator

OUTLINING SOLUTION ALGORITHM

In deriving the implicit Approximate Factorization Algorithm, Beam-Warming [1] in 1976 used the Euler temporal difference approximation [1],

$$Q^{n+1} = Q^n + \Delta t Q^n_t \tag{15}$$

Now equation (16) is inserted in equation (3) together with equation (5)and (6), which results in,

$$\left[I + \Delta t\left(\delta_{\varsigma}^{-}A^{+} + \delta_{\varsigma}^{+}A^{-} + \delta_{\eta}^{-}B^{+} + \delta_{\eta}^{+}B^{-}\right)\right]\Delta Q = -\Delta t * R^{n} \tag{16}$$

where

$$R^{n} = \delta_{\varsigma}^{-}E^{+} + \delta_{\varsigma}^{+}E^{-} + \delta_{\eta}^{-}F^{+} + \delta_{\eta}^{+}F^{-} \tag{17}$$

Solution can be obtained using the ADI method

NEW METHOD FOR BOUNDARY CONDITION IMPLEMENTATION IN TWO-DIMENSIONAL INVISCID FLOW

In the present subsection the new method of dealing with the flow boundary conditions and its implementation in the (FVS) for two-dimensional inviscid compressible flow is presented. Note that all the flow dependence relations for each boundary condition are listed in Appendix A.

1. Solid wall (tangency to η= cons. Line) (2-D)

If $\eta_y \succ \eta_x$, then the y momentum equation has a larger contribution to the normal momentum equation so the y momentum equation is dropped.

$$v = \frac{-\eta_x}{\eta_y} * u \tag{18}$$

$$\therefore \Delta Q_3 = \frac{-\eta_x}{\eta_y} * \Delta Q_2 \tag{19}$$

$$\frac{\partial \Delta Q_3}{\partial \Delta Q_2} = \frac{-\eta_x}{\eta_y} \tag{20}$$

Implementing the boundary condition can be summarized by the following procedure:
1 – Drop the Eq. at which Q_3 are in the temporal derivative term i.e. Eq. 3
2 – Modify the Jacobian matrices as follows,

$$A * \Delta Q = \begin{bmatrix} A_{11} & A_{12} & A_{13} & A_{14} \\ A_{21} & A_{22} & A_{23} & A_{24} \\ A_{31} & A_{32} & A_{33} & A_{34} \\ A_{41} & A_{42} & A_{43} & A_{44} \end{bmatrix} * \begin{bmatrix} \Delta Q_1 \\ \Delta Q_2 \\ \Delta Q_3 \\ \Delta Q_4 \end{bmatrix} \tag{21}$$

After modification, this becomes,

$$A*\Delta Q=\begin{bmatrix} A_{11} & A_{12}+A_{13}*\dfrac{\partial \Delta Q_3}{\partial \Delta Q_2} & A_{14} \\ A_{21} & A_{22}+A_{23}*\dfrac{\partial \Delta Q_3}{\partial \Delta Q_2} & A_{24} \\ A_{41} & A_{42}+A_{43}*\dfrac{\partial \Delta Q_3}{\partial \Delta Q_2} & A_{44} \end{bmatrix}*\begin{bmatrix} \Delta Q_1 \\ \Delta Q_2 \\ \Delta Q_4 \end{bmatrix} \quad (22)$$

$$B*\Delta Q=\begin{bmatrix} B_{11} & B_{12}+B_{13}*\dfrac{\partial \Delta Q_3}{\partial \Delta Q_2} & B_{14} \\ B_{21} & B_{22}+B_{23}*\dfrac{\partial \Delta Q_3}{\partial \Delta Q_2} & B_{24} \\ B_{41} & B_{42}+B_{43}*\dfrac{\partial \Delta Q_3}{\partial \Delta Q_2} & B_{44} \end{bmatrix}*\begin{bmatrix} \Delta Q_1 \\ \Delta Q_2 \\ \Delta Q_4 \end{bmatrix} \quad (23)$$

$$E=\begin{bmatrix} E_1 \\ E_2 \\ E_4 \end{bmatrix} \quad (24). \qquad F=\begin{bmatrix} F_1 \\ F_2 \\ F_4 \end{bmatrix} \quad (25)$$

The above modification is implemented into the FDE and the solution sequence $\Delta Q_1, \Delta Q_2, \Delta Q_4$ and then get $\Delta Q_3=\dfrac{\partial \Delta Q_3}{\partial \Delta Q_2}*\Delta Q_2$. (26)

If $\eta_x \succ \eta_y$ then the x-momentum equation has larger contribution to the normal momentum equation so the x-momentum equation is dropped.

The above modification is implemented in to the FDE and the solution sequence $\Delta Q_1, \Delta Q_3, \Delta Q_4$ then $\Delta Q_2=\dfrac{\partial \Delta Q_2}{\partial \Delta Q_3}*\Delta Q_3$ is obtained.

(27)

2. Inflow Boundary (2-D)

Case A: Supersonic Inflow

$$\begin{bmatrix} \Delta Q_1 \\ \Delta Q_2 \\ \Delta Q_3 \\ \Delta Q_4 \end{bmatrix}_{i=1}=\begin{bmatrix} 0 \\ 0 \\ 0 \\ 0 \end{bmatrix} \quad (28)$$

Case B: Subsonic Inflow

To = cons., Po =cons., v = u*tan (θ_{in})

Implementing the boundary condition can be summarized by the following procedure:

1– Drop the equations at which Q1, Q3, Q4, are in the temporal derivative term.

2– Modify the Jacobian matrices as follows,

apply the new methodology which has been discriped in detailes for the tangency boundary condition to get ΔQ_2 then;

$$\Delta Q_1 = \frac{\partial \Delta Q_1}{\partial \Delta Q_2} * \Delta Q_2$$
$$\Delta Q_3 = \frac{\partial \Delta Q_3}{\partial \Delta Q_2} * \Delta Q_2 \qquad (29)$$
$$\Delta Q_4 = \frac{\partial \Delta Q_4}{\partial \Delta Q_2} * \Delta Q_2$$

3. Out Flow Boundary (2-D)

Case A: Supersonic Out Flow

Use linear extrapolation,

$$\begin{bmatrix} Q_1 \\ Q_2 \\ Q_3 \\ Q_4 \end{bmatrix}_{imx} = 2 * \begin{bmatrix} Q_1 \\ Q_2 \\ Q_3 \\ Q_4 \end{bmatrix}_{i\max-1} - \begin{bmatrix} Q_1 \\ Q_2 \\ Q_3 \\ Q_4 \end{bmatrix}_{i\max-2} \qquad (30)$$

Case B: Subsonic Out Flow

Only the back pressure P_b is specified. So must drop one equation (the energy equation) and solve the continuity equation with the two Momentum equations.

After performing the two ADI steps, obtain $\Delta Q_1, \Delta Q_2, \Delta Q_3$ and hence ΔQ_4 is obtained from the relation,

$$\Delta Q_4 = \frac{\partial \Delta Q_4}{\partial \Delta Q_1} * \Delta Q_1 + \frac{\partial \Delta Q_4}{\partial \Delta Q_2} * \Delta Q_2 + \frac{\partial \Delta Q_4}{\partial \Delta Q_3} * \Delta Q_3 \qquad (31)$$

APPLICATIONS

The Numerical solution of the two-dimensional flow through convergent-divergent nozzle is presented. This section also includes a numerical solutions of the two-dimensional flow through turbomachine cascade. The steady state solution is reached when five order of magnitude as maximum error achieved.

1. Transonic Nozzle test case

In this test case the 2-D Euler solver developed is extended to deal with transonic flow through convergent-divergent nozzle. The nozzle geometry and back-pressure condition are given below:

Back Pressure: $\frac{P_b}{P_{o1}} = .75$

The geometry of the nozzle is described by the following function:

$$y_u = \begin{cases} (1.398 + .347 * \tanh(-.9 * x - 2)) & -5 \le x \le 0 \\ (1.398 + .347 * \tanh(.9 * x - 2)) & 0 \le x \le 5 \end{cases}$$

$$y_u = \begin{cases} -(1.398 + .347 * \tanh(-.9 * x - 2)) & -5 \le x \le 0 \\ -(1.398 + .347 * \tanh(.9 * x - 2)) & 0 \le x \le 5 \end{cases} \qquad (32)$$

The solution is obtained using an H-grid 51*30 in addition to a 51*5 " very coarse grid" with no orthogonality at the nozzle surface and with CFL = 1.5 for 700 iterations. Results are shown in figs (1) to (4).

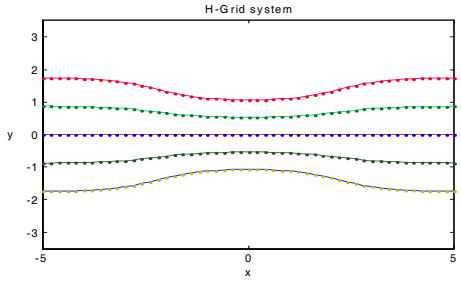

Figure (1) H-Grid 51*5

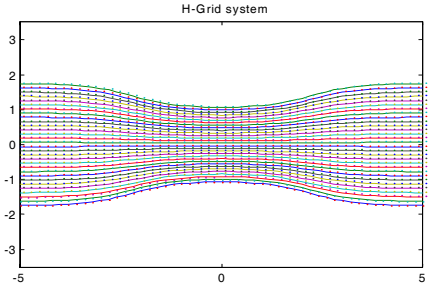

Figure (2) H-Grid 51*30

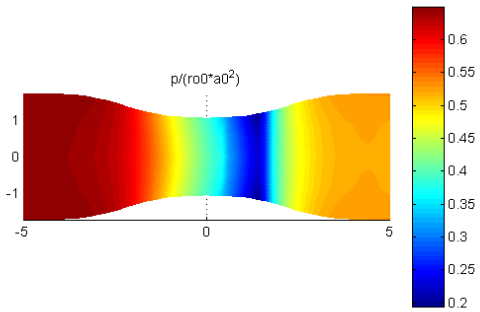

Figure (3) Pressure distribution (51*5 grid)

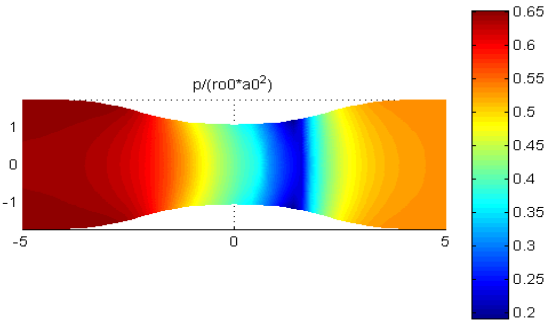

Figure (4) Pressure distribution (51*30 grids)

Figures show that there is a slight difference in the numerical solution (about 1.3%) of both cases. The disadvantage of the coarse grid is losing of the shock curvature.

2. Highly Non-Orthogonal Transonic Test Case

In this test case the 2-D Euler solver developed is extended to deal with transonic flow through convergent-divergent nozzle,

Back Pressure: $\frac{P_b}{P_{o1}} = .65$

The geometry of the nozzle is described by the following function:

$$y_u = \begin{cases} 2 & 0 \le x \le 0.5 \\ +(1.5+.5*\cos(x-0.5)*\frac{\pi}{2})) & 0.5 \le x \le 4.5 \\ 2 & 4.5 \le x \le 5 \end{cases}$$

$$y_l = \begin{cases} -2 & 0 \le x \le 0.5 \\ -(1.5+.5*\cos(x-0.5)*\frac{\pi}{2})) & 0.5 \le x \le 4.5 \\ -2 & 4.5 \le x \le 5 \end{cases} \qquad (33)$$

The solution is obtained using an H-grid 31*30 with no orthogonality at the nozzle surface and with a grid spacing in the η direction = 0.13 “coarse grid” with CFL = 1.5 for 1200 iterations and high non-orthogonality of the grid axis near nozzle surface.

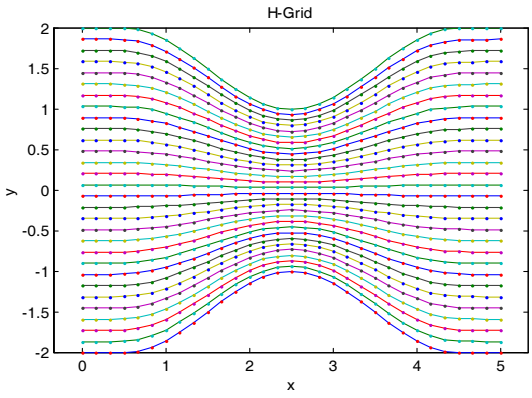

Figure (5) H-Grid 31*30

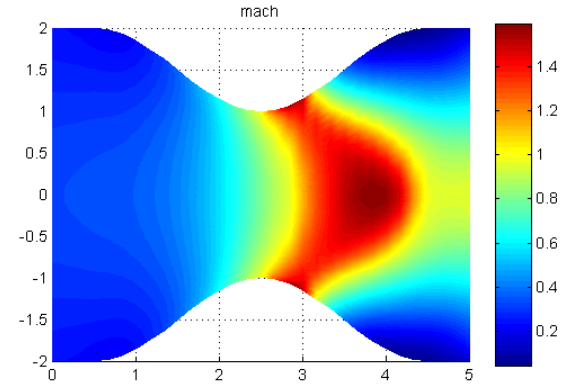

Figure (6) Mach distribution

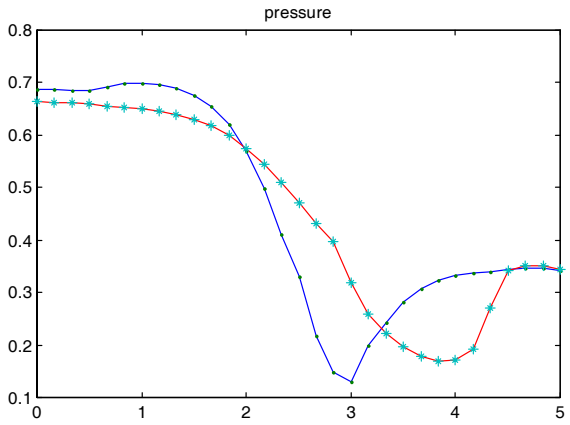

Figure (7) Pressure distribution “*” centerline, “-“ wall

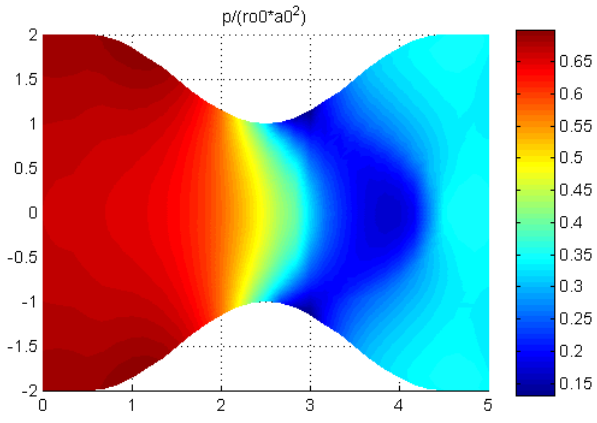

Figure (8) Pressure distribution

3. Cascade Test Cases

In this section, the solution of highly subsonic and transonic inviscid compressible flow is presented versus the experimental tests available for HIGH CAMBERED DCA CASCADE [9]. The comparison will be based on the Mach distribution on the blade surfaces excluding the leading and trailing edges because it is not available in the experimental data.

3.1. Highly Subsonic Test Case M1= .64

In this test case the inviscid compressible solution is obtained numerically using Euler's two-dimensional flow model and comparison with experiment shows good agreement but with deviation from experimental values just after the separation bubble at the blade leading edge. It also shows deviation from experimental values after the maximum Mach number point due to the absence of the boundary layer displacement thickness in the inviscid calculations.

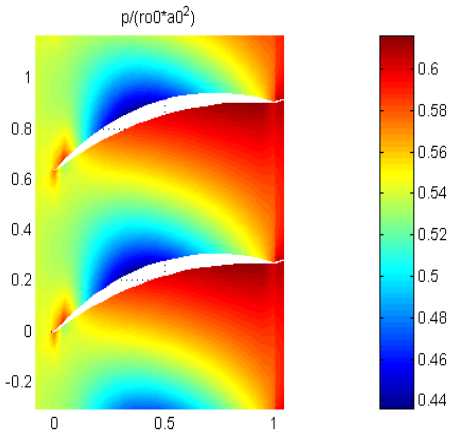

Figure (9) Pressure distribution

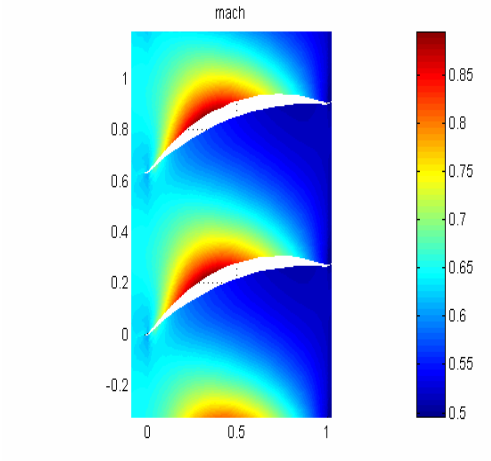

Figure (10) Mach Number distribution

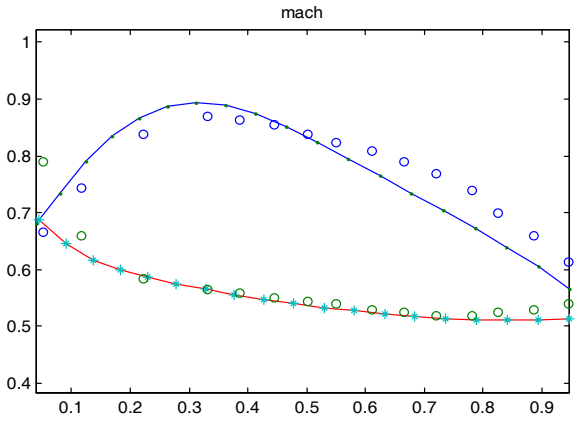

Figure (11) Mach distribution, "*" & "." Numerical, "O" Experimental Ref [9]

Results show a deviation between the computed Mach number distribution and the experimental values at the blade lower surface leading edge and after the maximum Mach number point on the upper surface. The deviation at the leading edge of the blade lower surface is due to sharp edge approximation of the leading edge. The deviation after the maximum Mach number point at the blade upper surface may be due to the absence of the boundary layer displacement thickness in the inviscid calculations.

CONCLUSION

An approximate factorization procedure coupled with flux vector splitting methods, proposed by Van Leer and Steger-Warming, has been implemented to solve two-dimensional Euler's flow model. The developed solver is found to be useful to get accurate results with very limited computing facilities (microcomputers). The new treatment of the flow boundary conditions implemented here has enabled the use of a very coarse computational grid which dramatically reduce the amount of memory used and the computation time.

Two-Dimensional Nozzle Flow

The Two-Dimensional Euler's flow solver has succeeded to solve multi-sonic flow regimes. The transonic test case shows the success of the inflow and out flow boundary conditions and at each test case presents a success in tangency boundary condition implementation. The transonic test case shows a sharp presentation of the shock wave and accuracy in locating the shock wave. The highly non-orthogonal grid test case shows the ability of the developed solver to obtain solution even with bad grid point distribution and the results show a sharp resolution of the shock wave without any dispersion in its location. The results of each test case show a very good agreement with the analytical results. The grid spacing normal to the boundary surface and achieved in this study was estimated to be fifty times larger than the recommended values by some researchers

Two-Dimensional Cascade Flow

The computed Mach number distribution is compared with the experimental values and shows a deviation between both values at the blade lower surface of the leading edge and after the maximum Mach number point on the upper surface. Good agreement is obtained at the remaining points. The deviations at the blade lower surface of the leading edge are due to the formation of the separation bubble which is not appear in the inviscid calculations. The deviations after the maximum Mach number point on the upper surface may be due to the absence of the boundary layer displacement thickness in the inviscid calculations. Other test cases are presented in order to examine the ability of the developed solver to analyze subsonic and transonic flows through turbomachine cascade. The transonic test case shows a sharp resolution of the shock wave that appears only on the blade upper surface.

Acknowledgment

The author would like to thank **Dr M.M. Abdelrahman** for his continuous effort and guidance through this research, the author would like to acknowledge the **Airforce Commandant**, Chairman of research and development department **Gen. Dr. Abdullah EL Ramsisy**, **Col. Dr. Mohamed Ibraheem** For their continuous engorgements during this researches.

REFERENCES

1- John D. Anderson, Jr. "Computational Fluid Dynamics, The basic with applications", McGraw-Hill, Inc., New York 1995.

2- Anderson, W. K., Thomas, J. L. and Whitfield, D. L., "Three Dimensional Multigrid Algorithms for the Flux-Split Euler Equations", NASA Technical Paper 2829, Nov. 1988.

3- Jameson, A., Schmidt, W., and Turkel, E., "Numerical Solution of the Euler Equations by Finite Volume Method Using Runge Kutta Time Stepping Schemes", AIAA Paper 81-1259, June 1981.

4- Steger, J. L., and Warming, R. F., "Flux-Vector Splitting of the inviscid Gas Dynamic Equations With Application to Finite Difference Methods", Journal of Computational Physics, Vol. 40, 1981.

5- Anderson, W. K., Thomas, J. L. and Van-Leer, B., "A Comparison of Finite Volume Flux Vector Splitting for Euler Equations", AIAA Paper 85-0122, Jan. 1985.

6- Van Leer, B., "Flux-Vector Splitting for the Euler Equations", Lecture Note in Physics, Vol. 170, 1982.

7- Abdelrahman M., "An Implicit Time-Marching Method for the calculation of Transonic Flows using Euler Equations", Fourth International Conference for Mechanical Power Engineering, Cairo, October 1982.

8- Hoffman, A. K., "Computational Fluid Dynamics", Engineering Education System, 1989.

9- Von Karman Institute for Fluid Dynamics, " Transonic Flow In Turbomachinary ", Lecture series 59 Vol. 2, May. 1973.

10- Thompkins, W. T., Oliver, D. A., "Three-Dimensional Flow Calculation For A Transonic Compressor Rotor", AGARD-CP-195, 5 May. 1977.

11- Gopalakrishnan, S., Bozzola, R., "A Numerical Technique for the Calculation of Transonic Flows in Turbomachinary Cascades", Gas Turbine Conference & Products Show, Houston, Texas, March 28-April 1, 1971.

12- Mohammad Baher Azab, "On The Numerical Solution Of Three-Dimensional Transonic Inviscid Internal Flow problems With Application To Centrifugal Compressor ", Master Thesis, Aerospace department, Cairo university 2002.